

## ANISOTROPY SIGNATURES OF SOLAR ENERGETIC PARTICLE TRANSPORT IN A CLOSED INTERPLANETARY MAGNETIC LOOP

A. SÁIZ,<sup>1</sup> D. RUFFOLO,<sup>1</sup> J. W. BIBER,<sup>2</sup> P. EVENSON,<sup>2</sup> AND R. PYLE<sup>2</sup>

Received 2007 February 14; accepted 2007 September 13

### ABSTRACT

Recent studies have stressed the importance of solar energetic particle (SEP) transport under disturbed interplanetary conditions, including the case of detection inside a closed interplanetary magnetic loop ejected by a preceding solar event. In this case, particles might be observed to arrive from the far leg of the loop, thus arriving at the detector while traveling sunward. We perform numerical simulations of the focused transport of SEPs along Archimedean spiral and magnetic loop configurations. For loop configurations, we consider injection along either the near leg or the far leg of the loop, either with or without compression at the leading edge. We show that there are specific anisotropy signatures of transport in a closed magnetic loop configuration. SEPs traveling sunward cannot have a high, sustained anisotropy due to the effect of inverse focusing. As an example, the relativistic SEP event of 2003 October 28 exhibited unusual directional distributions, with an early peak of particle flow  $\approx 120^\circ$  and a main peak  $\approx 80^\circ$  from the radial direction. However, quantitative fitting of data from the SpaceShip Earth network of polar neutron monitors indicates that injection along the far leg of an interplanetary loop is not a good description; our analysis strongly favors transport from the Sun to the Earth over a short path length of  $\sim 1$  AU.

*Subject headings:* interplanetary medium — methods: numerical — solar-terrestrial relations — Sun: coronal mass ejections (CMEs) — Sun: particle emission

### 1. INTRODUCTION

There is sufficient understanding of the transport of solar energetic particles (SEPs) in the interplanetary medium that it is now possible to model those processes accurately (Ruffolo 1995; Hatzky et al. 1997; Lario et al. 1998; Kocharov et al. 1998) and to fit data to infer transport conditions and the time dependence of injection near the Sun (Ruffolo et al. 1998; Bieber et al. 2002). Originally such work concentrated on an Archimedean spiral magnetic field configuration, as expected for an unperturbed solar wind due to the rotation of the Sun. However, recent studies have stressed the importance of particle transport in disturbed magnetic field configurations, such as magnetic bottlenecks (Bieber et al. 2002), closed interplanetary magnetic loops, including interplanetary flux ropes (Torsti et al. 2004; Kocharov et al. 2005, 2007; Ruffolo et al. 2006), and other low-beta plasma structures (Buttighoffer 1998; Buttighoffer et al. 1999; Reames et al. 2001). Magnetic bottlenecks comprise open field lines that are locally compressed due to a preceding coronal mass ejection (CME), especially on the western flank of the CME (Cane 1988). Major particle events frequently occur as part of a series of events from one active region, so it is not unusual for a solar event to occur to the west (in the direction of solar rotation) of a preceding CME. Closed interplanetary magnetic loops can occur within magnetic clouds, which are found in some CME ejecta, so these can again result from a preceding CME. The presence of such structures can profoundly affect the inferred timing of particle injection at the Sun, which in turn has important implications for the physics of solar particle acceleration (e.g., Kahler 2005; Manchester et al. 2005).

As scientific interest is focusing more on transport in disturbed interplanetary field conditions, closed interplanetary magnetic

loops are increasingly invoked to explain unusual time-density or directional distributions of SEPs from observations. Indeed, it can be difficult to determine whether or not the local magnetic field line is connected to the Sun on both ends at the time of detection of energetic particles. In some cases independent confirmation is available, e.g., from magnetic field and plasma data that indicate a magnetic cloud (Burlaga et al. 1981) and bidirectional flows of suprathermal or energetic particles from the Sun (Palmer et al. 1978; Bame et al. 1981; Richardson & Cane 1996) that indicate magnetic connection to the Sun at both ends of a loop. Similarly, Bieber et al. (2002) inferred a magnetic bottleneck beyond the Earth in order to obtain a better fit to relativistic solar particle observations, and the bottleneck was confirmed by magnetic field data and, later on, by fortuitous observations of the magnetic cloud by the *NEAR* spacecraft (Mulligan et al. 2005). A loop configuration was used to explain the large event on 1989 September 29 (see the review by Miroshnichenko et al. 2000), but the loop in this event was more difficult to confirm. Although no magnetic or plasma data were available for the event of 1989 October 22, Ruffolo et al. (2006) had some confirmation of a loop configuration, that is, a bidirectional flux of galactic cosmic rays (GCRs) during the Forbush decrease immediately before the solar event, which can be associated with closed magnetic structures (see also Richardson et al. 2000). To quantitatively fit the directional distribution of relativistic solar protons as a function of time, Ruffolo et al. (2006) required injection along both legs of the loop, including the effect of adiabatic focusing (also known as magnetic mirroring) near the Sun.

Loops have also been invoked to explain the transport of relativistic solar particles from an important solar event on 2003 October 28. This event, whose X17-class X-ray flare peaked at 11:10 UT at a derived position of  $18^\circ\text{S } 20^\circ\text{E}$  (EIT High Cadence Wavelength),<sup>3</sup> had significant space weather effects specifically due to the prompt arrival of SEPs at Earth. The prompt, intense

<sup>1</sup> Department of Physics, Faculty of Science, Mahidol University, Bangkok 10400, Thailand.

<sup>2</sup> Bartol Research Institute and Department of Physics and Astronomy, University of Delaware, Newark, DE 19716.

<sup>3</sup> From the SolarSoft web site, [http://www.lmsal.com/solarsoft/latest\\_events\\_archive.html](http://www.lmsal.com/solarsoft/latest_events_archive.html).

high-energy particle flux, characteristic of events like this, plays a role in space weather effects on human activities in space and at high altitude in Earth's atmosphere, especially in polar regions. For example, the prompt component of SEPs can account for the majority of satellite failures associated with the event of 2003 October 28 (L. Barbieri 2004, private communication) and in general poses a key radiation hazard to astronauts and air crews (Wilson et al. 2003). SEPs would normally be expected to preferentially move anti-sunward along magnetic field lines until interplanetary scattering isotropizes their directional distribution. However, both Bieber et al. (2005) and Miroshnichenko et al. (2005) presented evidence for unusual directional distributions of relativistic solar particles, with an early peak of particles beamed roughly sunward, followed by a main peak directed northward, or nearly  $90^\circ$  to the nominal Parker spiral direction (Parker 1958).

These papers discussed the possibility of a closed interplanetary magnetic loop to explain some of these features, specifically concerning the early peak, the main peak, and the slow decay of SEP density with time. However, subsequent plasma and magnetic field observations indicate that while there was a magnetic cloud as part of a preceding CME, that field structure actually passed Earth before the onset of this event (Mulligan et al. 2005).

In the present work we use quantitative modeling to examine whether transport in an interplanetary loop has other observable effects that can be used to confirm or refute the loop hypothesis. We numerically solve an equation of focused transport of SEPs along Archimedean spiral and magnetic loop configurations, including for the first time a loop that is continuously compressed near its leading edge. There are distinctive anisotropy signatures of transport in a closed magnetic loop configuration. In particular, when a beam of particles moves along the far leg of an interplanetary loop and then proceeds along the near leg back toward the Sun, the beam must be significantly decollimated by the effect of adiabatic focusing (Roelof 1969). Thus, the loop hypothesis must be used with care. As an example, we demonstrate by quantitative fitting of data from the Spaceship Earth network of polar neutron monitors that the main peak of relativistic solar particles during the 2003 October 28 event is not consistent with injection along the far leg of a closed interplanetary magnetic loop. Instead, our analysis strongly favors transport from the Sun directly to the Earth over a short path length of  $\sim 1$  AU. We discuss possible explanations of the unusual aspects of this event in the context of these new results.

## 2. TRANSPORT MODEL

In order to understand the expected features of a SEP distribution propagating in a magnetic loop, we numerically solve a Fokker-Planck equation of pitch-angle transport. Following Ng & Wong (1979), we define the particle distribution function  $F$  depending on time,  $t$ , pitch-angle cosine,  $\mu$ , distance from the Sun along the interplanetary magnetic field,  $z$ , and momentum,  $p$ , as

$$F(t, \mu, z, p) \equiv \frac{d^3 N}{dz d\mu dp}, \quad (1)$$

where  $N$  represents the number of particles inside a given flux tube. In this work we are interested in the transport of relativistic protons, for which the velocity is much greater than both the CME speed and the solar wind speed. Thus, we neglect the solar wind speed and consider a static magnetic configuration along which the SEPs stream. We will not model the evolution of the SEP distribution at late times in the event, so any change in the magnetic cloud's size or position can be neglected. We can then treat the

loop configuration with some generality, since we do not need to specify the exact shape of the magnetic field line. An equation of focused transport can then be expressed as (Ruffolo 1991)

$$\begin{aligned} \frac{\partial F(t, \mu, z, p)}{\partial t} &= -\frac{\partial}{\partial z} \mu v F(t, \mu, z, p) && \text{(streaming)} \\ &- \frac{\partial}{\partial \mu} \frac{v}{2L(z)} (1 - \mu^2) F(t, \mu, z, p) && \text{(focusing)} \\ &+ \frac{\partial}{\partial \mu} \frac{\varphi(\mu)}{2} \frac{\partial}{\partial \mu} F(t, \mu, z, p) && \text{(scattering)}. \end{aligned} \quad (2)$$

The particle velocity is denoted by  $v$ , the focusing length by  $L(z) = -B/(dB/dz)$  (where  $B$  is the magnitude of the magnetic field), and the pitch-angle scattering coefficient by  $\varphi(\mu)$ . Our numerical solutions of a related transport equation (Ruffolo 1995) have been reproduced by several other authors (Hatzky et al. 1997; Lario et al. 1998; Kocharov et al. 1998; Nutaro et al. 2001). The present work uses the numerical method of Nutaro et al. (2001).

The pitch-angle scattering is parameterized as  $\varphi(\mu) = A|\mu|^{q-1} \times (1 - \mu^2)$ . This expression was originally derived in the context of quasi-linear scattering theory (Jokipii 1971; Earl 1973), and here we employ this as a convenient parameterization. The amplitude  $A$  is related to the parallel scattering mean free path  $\lambda \equiv 3D/v$  through the diffusion coefficient

$$D = \frac{v^2}{4} \int_{-1}^1 \frac{(1 - \mu^2)^2}{\varphi(\mu)} d\mu, \quad (3)$$

so  $\lambda \propto 1/A$ . The scattering parameter  $q$ , representing the spectral index of magnetic fluctuations in interplanetary turbulence, is taken to be 1.0 (see § 4).

As can be seen in equation (2), the most relevant processes in relativistic SEP transport are the streaming, pitch-angle scattering, and adiabatic focusing (Roelof 1969). As pointed out by Kocharov et al. (1996), the effects of focusing are important in every situation, including situations of very low scattering as well as strong scattering.

We consider six magnetic configurations in which to model SEP transport (Fig. 1). In configuration 1, we assume that the magnetic field line connecting the Earth with the SEP acceleration site at the Sun is an Archimedean spiral driven by a solar wind speed  $v_{sw}$  of  $800 \text{ km s}^{-1}$ , so the path length is  $z = 1.03 \text{ AU}$  (Bieber et al. 2005). In configuration 2, we assume that the field line connects with the acceleration site along a much longer Archimedean spiral field line, with  $z = 2.2 \text{ AU}$ , as a baseline run for comparison with configurations 4 and 6 (see below); an Archimedean spiral field line of this length would result from a (completely unrealistic) value of the solar wind speed of  $114 \text{ km s}^{-1}$ .

The definition of the focusing length  $L$  depends on the configuration of the interplanetary magnetic field. For the Archimedean spiral configurations, we have

$$L = \frac{r(r^2 + R^2)^{3/2}}{R(r^2 + 2R^2)}, \quad (4)$$

where  $R = v_{sw}/(\Omega \cos \theta)$ ,  $\Omega$  is the sidereal angular frequency of solar rotation (derived from a synodic period of 26.75 days; Bai 1987), and  $\theta$  is the Earth's heliolatitude with respect to the solar equator (Ruffolo et al. 2006).

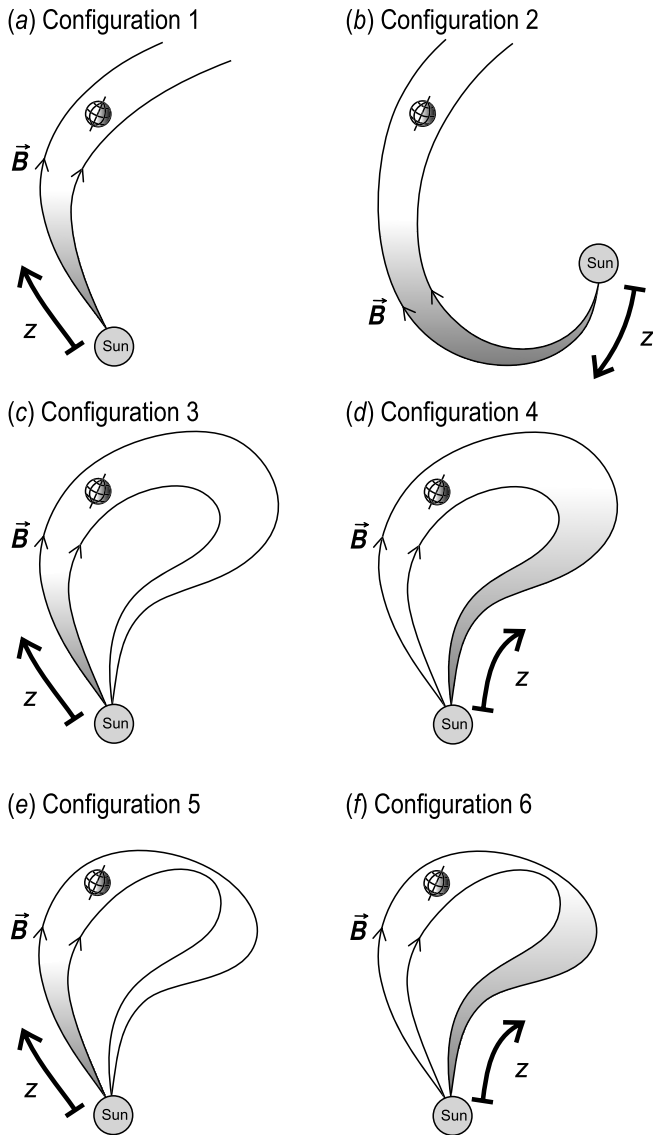


FIG. 1.— Schematic display of the six configurations of the interplanetary magnetic field considered in this work. (a) Configuration 1, the usual Archimedean spiral with path length 1.03 AU from the Sun to the Earth. (b) Configuration 2, an Archimedean spiral of path length 2.2 AU. (c–d) Configurations 3 and 4, a simple (uncompressed) interplanetary magnetic loop that connects the Earth to a SEP acceleration site along the near leg (path length 1.03 AU) or far leg (path length 2.2 AU), respectively. (e–f) Configurations 5 and 6, similar to configurations 3 and 4 but for a compressed loop. The distance  $z$  is defined for each configuration as indicated. Shading of the magnetic flux tube shows the presence of SEPs some time after their injection but before their arrival to Earth.

Next, we consider simple (uncompressed) loop models. In configuration 3, SEPs arrive from the Sun along one leg of an interplanetary magnetic loop, traveling the same distance as in configuration 1, i.e.,  $z = 1.03$  AU, while in configuration 4 we assume that the field line that connects with the acceleration site is the far leg of a loop, again with  $z = 2.2$  AU (as suggested by Miroshnichenko et al. 2005). In both configurations 3 and 4, the total length of the loop is  $\ell = 3.23$  AU.

For a simple loop of total length  $\ell$ , we can roughly model  $L$  using a function that is symmetric around the midpoint of the loop and appropriate for radial magnetic field lines close to the Sun on both ends. Note that

$$\frac{1}{L} = -\frac{d \ln B}{dz}. \quad (5)$$

Thus, for the case of a loop in which the field line has the same value of  $B$  at the start and end points, the integral of  $1/L$  along  $z$  must be zero. If the function is chosen to be odd around the midpoint, that condition is fulfilled. We use (Bieber et al. 2005; Ruffolo et al. 2006)

$$L(z) = \frac{\ell}{2\pi} \tan\left(\frac{\pi z}{\ell}\right), \quad (6)$$

which means that the magnetic field is

$$B(z) \propto \csc^2\left(\frac{\pi z}{\ell}\right). \quad (7)$$

The form of the focusing length used in configurations 3 and 4, equation (6), implies that the magnetic field is weakest at the center point of the loop. However, it might be argued that a real interplanetary loop is compressed at its leading edge when traveling faster than the ambient solar wind (Vandas et al. 2002; Manchester et al. 2005; Kocharov et al. 2007), which makes the magnetic field stronger there. In such a compressed loop, the sign of the focusing may change, relative to the uncompressed case, when particles enter or exit the compressed region. The strong variation in focusing could have a substantial effect on the particle transport.

To explore this possibility we develop a model of a continuously compressed loop. Configurations 5 and 6 are similar to configurations 3 and 4, respectively, except that the focusing length  $L(z)$  is now set to

$$L(z) = \frac{\ell}{2\pi} \frac{\tan(\pi z/\ell)}{\cos(2\pi z/\ell)}, \quad (8)$$

so that

$$B(z) \propto \csc^2\left(\frac{\pi z}{\ell}\right) \exp\left[-2 \cos^2\left(\frac{\pi z}{\ell}\right)\right]. \quad (9)$$

In comparison with the simple loop (eq. [7]), we see that  $B$  in this compressed loop model has a broad peak near the midpoint  $z = \ell/2$  due to the exponential term. For equal  $B$  values near the Sun, our compressed loop has a field at the midpoint that is  $\approx 7$  times stronger than that of the uncompressed loop. The focusing length  $L$  is positive for  $z$  between 0 and  $\ell/4$  and again between  $\ell/2$  and  $3\ell/4$ , and negative in the other intervals. For configuration 5 we use a short path length ( $z = 1.03$  AU), and for configuration 6 we use a long path length ( $z = 2.2$  AU). In both cases  $\ell = 3.23$  AU, and the observer is actually located in a region of sunward focusing.

### 3. EVOLUTION OF THE SOLAR PARTICLE DIRECTIONAL DISTRIBUTION

The combined effects of the path length and the scattering coefficient on the SEP transport are clearly exemplified by numerical simulations of the transport of SEPs after an instantaneous injection near the Sun, and examining the expected density and anisotropy at Earth. In Figure 2 we show the evolution of the distribution function of SEPs in position  $z$  and pitch-angle cosine  $\mu$  for the different magnetic configurations considered. For comparison purposes, we use a higher mean free path of interplanetary scattering for cases with a longer path length.

We use various quantities to describe the directional distribution and its anisotropy.

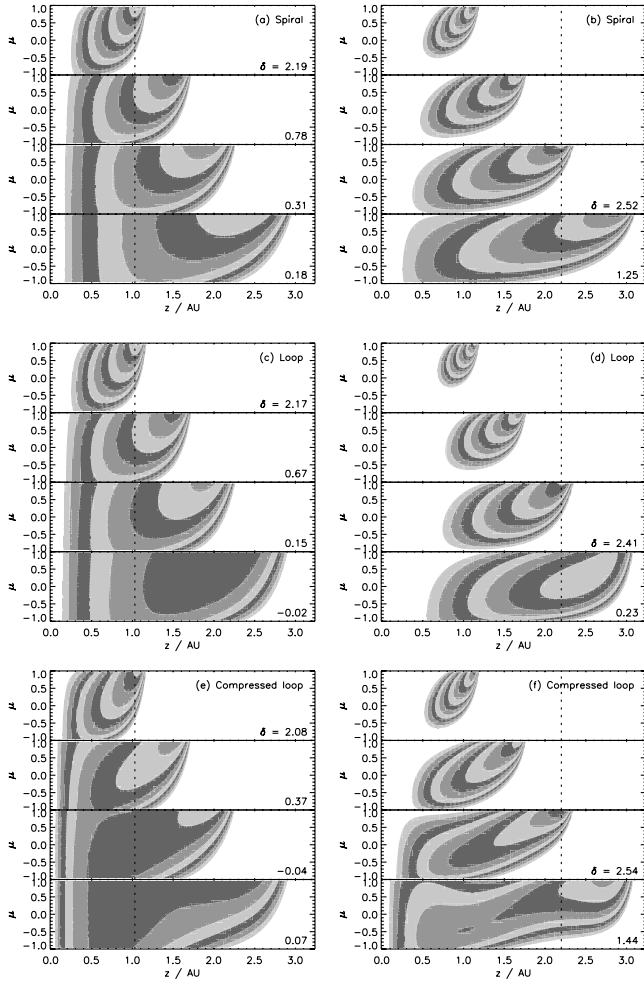


FIG. 2.— Evolution of the distribution function  $F$  in distance along the field line,  $z$ , and pitch-angle cosine,  $\mu$ , for 2.0 GeV protons in all six configurations, after an instantaneous injection near the Sun. For configurations 1 (panel a), 3 (panel c), and 5 (panel e), we use  $\lambda = 0.8$  AU. For configurations 2 (panel b), 4 (panel d), and 6 (panel f),  $\lambda = 2.4$  AU. Each panel shows (from top to bottom) the times  $t = 11, 16, 21$ , and 28 minutes after the injection. Contours in  $F$  are logarithmically spaced, with three contours representing an increase in  $F$  by a factor of 10. Shading of the contours is added for clarity only, and  $F$  is always higher at smaller contours in each panel, starting from the same minimum threshold (unshaded areas). The dotted line indicates the position of the Earth for each configuration. The value of the dipole anisotropy  $\delta$  at the position of the Earth is indicated where applicable. In all panels,  $z = 0$  is at the Sun, while for loop configurations, (c–f), the maximum value of  $z$  is also at the Sun. These results demonstrate that for loop configurations, there is strong reverse focusing and a rapid decrease in dipole anisotropy as particles move back toward the Sun at high  $z$ , although this effect may be suppressed temporarily if particles traverse a compressed region.

Density:

$$f_0 \equiv \frac{1}{2} \int_{-1}^1 F(\mu) d\mu, \quad (10)$$

the average of the distribution function over the pitch-angle cosine  $\mu$  and the coefficient of  $P_0(\mu)$  in a Legendre expansion of the distribution function. This can also be called the omnidirectional density (or intensity).

Weighted anisotropy:

$$f_1 \equiv \frac{3}{2} \int_{-1}^1 \mu F(\mu) d\mu, \quad (11)$$

the coefficient of  $P_1(\mu)$  in a Legendre expansion. This can also be called the first-order anisotropy, and it is a characteristic slope of  $F(\mu)$ . Physically, it represents the outflow of particles from the Sun minus the inflow.

Dipole anisotropy:

$$\delta \equiv \frac{f_1}{f_0} = 3\langle\mu\rangle, \quad (12)$$

where the average is weighted by the particle distribution function. Thus,  $-3 \leq \delta \leq 3$ . This is often simply called the “anisotropy.” It depends on the form of the directional distribution and not on the overall density of particles.

Curvature:

$$f_2 \equiv \frac{5}{2} \int_{-1}^1 \left( \frac{3}{2} \mu^2 - \frac{1}{2} \right) F(\mu) d\mu, \quad (13)$$

the coefficient of  $P_2(\mu)$  in a Legendre expansion. Also called the second-order anisotropy, this represents the curvature of  $F(\mu)$ .

For each magnetic configuration, the rapidly decreasing field near the Sun ( $B \propto 1/r^2$ ) leads to strong focusing (i.e., a low value of  $L$ ). Thus, particles are strongly focused near the Sun to form a “coherent pulse” (Earl 1976) regardless of their pitch-angle distribution at injection (Ruffolo & Khumlumert 1995). In this stage,  $F$  is concentrated in a highly anisotropic beam at high  $\mu$ , corresponding to a low pitch angle.

After the pulse has traveled a substantial fraction of a mean free path, the distribution function  $F$  evolves to a “wake” at lower  $\mu$  due to interplanetary scattering. At times and positions where the distribution function is spread over positive and negative values of  $\mu$ , the SEP anisotropy would be small. The value of the dipole anisotropy  $\delta$  is indicated at the position of the Earth in Figure 2. For other locations, the reader can visually estimate the dipole anisotropy from the relation  $\delta = 3\langle\mu\rangle$ .

The results shown in Figure 2 for Archimedean spiral configurations 1 and 2 are well-known effects of interplanetary transport and serve as “control runs” for the loop configurations. Note that for the Archimedean spiral configurations, where the focusing length  $L > 0$ , we obtain similar profiles of density and anisotropy for cases of lower or higher path length  $z$  by setting a lower or higher mean free path,  $\lambda$ . In other words, the isotropization of the SEP beam over long distances can be reduced by simply reducing the scattering. In a spiral configuration the density at a given location will monotonically decrease at late times.

Configuration 3 gives results at early times like those of configuration 1, showing that the initial evolution of the SEP distribution depends much more strongly on the scattering, focusing, and path length between the Sun and Earth than on the configuration beyond Earth. For late times the effects of the loop are noticeable, as particles encounter the region of negative focusing and are partially mirrored back to Earth, resulting in a slightly higher SEP density and much lower dipole anisotropy than for the spiral case. At even longer times (not shown in Fig. 2), the distribution function  $F$  in any loop configuration oscillates back and forth along the loop, especially if the scattering mean free path  $\lambda$  is very long, which at times may produce negative values of the dipole anisotropy. Therefore, a decrease in the dipole anisotropy  $\delta$  after the first arrival of SEPs is not avoided in the cases of very low scattering, but is in fact enhanced. At late times, and in absence of particle escape processes, the distribution will evolve to an equilibrium state, in which the density remains constant (in contrast with spiral

configurations) due to SEPs being trapped and mirroring back and forth in the loop.

On the other hand, for configuration 4, the transport along the far leg of a loop exhibits a systematic decollimation of the beam (in addition to that due to scattering) caused by the negative value of  $L$  (reverse focusing) as soon as the beam starts traveling back toward the Sun. This happens before the SEPs arrive to Earth, not afterward as in configuration 3. Thus, the effects of reverse focusing are noticeable immediately after the initial arrival of SEPs. Note in Figure 2 how the numerical value of the dipole anisotropy  $\delta$  at Earth drops very rapidly with time for this configuration 4.

For the compressed loop configurations, there is reverse focusing between  $\ell/4$  and  $\ell/2$ . In configuration 5, where the Earth is in the reverse focusing regime, the dipole anisotropy declines much more rapidly than for configurations 1 and 3. For configuration 6, the SEPs arriving at Earth have traveled through most of the compressed region of the loop, and the Earth is in the second region of positive focusing (between  $\ell/2$  and  $3\ell/4$ ). In addition, particles with low  $\mu$  are reflected by the compression, so the distribution observed at Earth comprises mostly SEPs “selected” to have small pitch angles. These two effects produce a high initial dipole anisotropy, as can be seen in Figure 2, but this decreases soon thereafter, as reverse focusing near the Sun jumps into the scene.

In Figure 3 we show the evolution with time of the first-order and second-order anisotropy (normalized by the density) in the three configurations with a long path length ( $z = 2.2$  AU). The spiral configuration 2 exhibits a relatively gradual decline in the dipole anisotropy  $f_1/f_0$ , which stabilizes near a small but positive value after 60 minutes. Such a gradual decline in the dipole anisotropy to a small, positive value is typically found in observed data. At the same time, there is a rapid decline in  $f_2/f_0$  to negative values, which indicates a negative curvature of  $F(\mu)$  as the bulk of the particles pass the Earth, followed by a gradual convergence to zero.

In the simple loop configuration 4, the dipole anisotropy  $f_1/f_0$  decreases more rapidly just after the time of onset and remains negative for some time before oscillating back to positive values. In the compressed loop configuration 6 the initial decrease is slower (and comparable to that in the spiral configuration 2), but after about 15 minutes from the onset time the dipole anisotropy falls steeply to negative values as in configuration 4. Such a 180° reversal in flow direction is not commonly observed in SEP data (although there have been observations of bidirectional flows, attributed to particle injection along both legs of the loop).

According to the lower panel of Figure 3, injection along the far legs of loops in configurations 4 and 6 leads to oscillations of the ratio  $f_2/f_0$ . Note, however, that the simulation results shown in Figures 2 and 3 are based on instantaneous particle injection near the Sun. In order to fit observed data, the simulation results for  $f_i$  must be convolved with the injection function, which is frequently of duration  $\geq 10$  minutes. Thus, one might expect the more rapid oscillations in Figure 3 to be washed out. The most robust signature of the reverse focusing in loops is the rapid decline in the dipole anisotropy soon after onset.

The reverse focusing effect in configurations 4 and 6 cannot be counterbalanced by a different scattering coefficient. Even assuming almost scatter-free conditions, the effects of reverse focusing do not disappear. In fact they become more evident, because the mirroring of the whole SEP distribution produces negative anisotropies, which would never happen in spiral configurations, with positive  $L$ . We can say that scatter-free transport is rare for ions, but focusing-free transport is simply impossible.

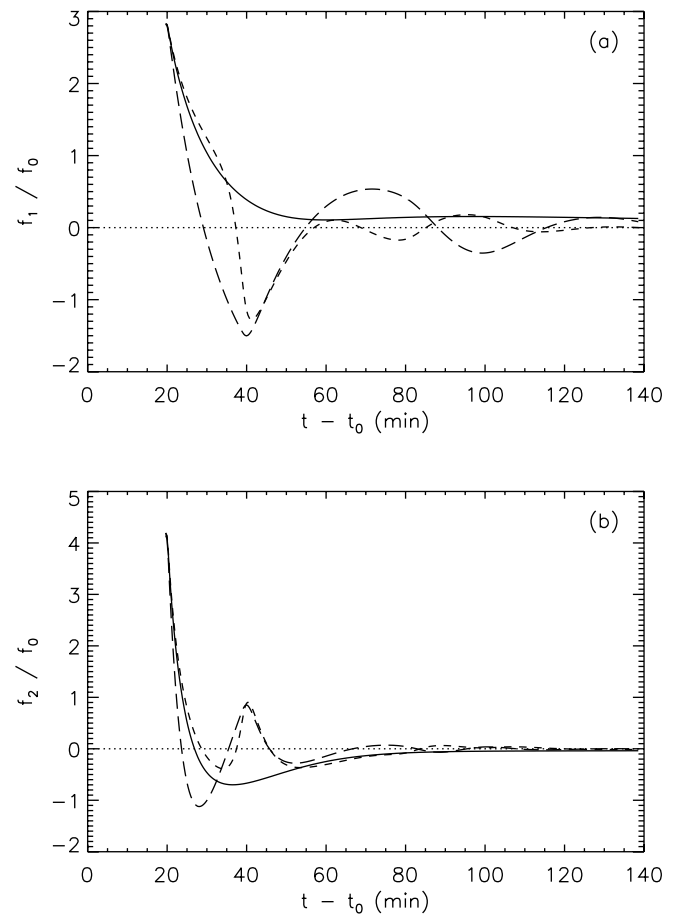


FIG. 3.—Evolution of two measures of the particle anisotropy from ratios of Legendre coefficients. (a) The dipole anisotropy  $f_1/f_0$  and (b)  $f_2/f_0$  for an extended spiral (configuration 2; solid line), loop (configuration 4; long-dashed line), and compressed loop (configuration 6; short-dashed line) after instantaneous injection of 2.0 GeV protons near the Sun at time  $t = t_0$ , for a scattering mean free path  $\lambda = 2.4$  AU. The proton injection is along the far leg of the loop configurations, and in each case the magnetic path length to the observer is 2.2 AU. The dotted line shows  $f_1 = 0$  and  $f_2 = 0$ . Both  $f_1$  and  $f_2$  oscillate between positive and negative values in the loop configurations before decaying, as the particle distribution is reflected back and forth by the focusing (magnetic mirroring) near the Sun at both ends of configurations 4 and 6, and at the compression region of configuration 6 only. When convolved with an extended injection function, the key observable indicator of transport along the far leg of a loop is the rapid decrease in the dipole anisotropy  $f_1/f_0$  soon after onset.

#### 4. APPLICATION TO THE SOLAR EVENT OF 2003 OCTOBER 28

In § 3 we showed that transport of SEPs from the far leg of a closed interplanetary magnetic loop should have observable anisotropy signatures. We now provide an example of how the absence of these signatures can refute the hypothesis of transport from the far leg of a loop. So far we have presented simulations for an instantaneous injection of particles near the Sun, but proper quantitative modeling of a specific event requires that we determine the actual time profile of injection. Thus, we fit the data in order to find acceptable magnetic configurations and the optimal injection function, as well as the optimal scattering mean free path. As an example, we perform this procedure for the main peak of the ground level enhancement (GLE) of 2003 October 28, for each of the assumed magnetic configurations, by using a linear  $\chi^2$ -minimization method.

The data used in the fits are time profiles of SEP density ( $f_0$ ), weighted anisotropy ( $f_1$ ), and curvature ( $f_2$ ), as constructed from the individual time profiles of 13 polar neutron monitor (NM)

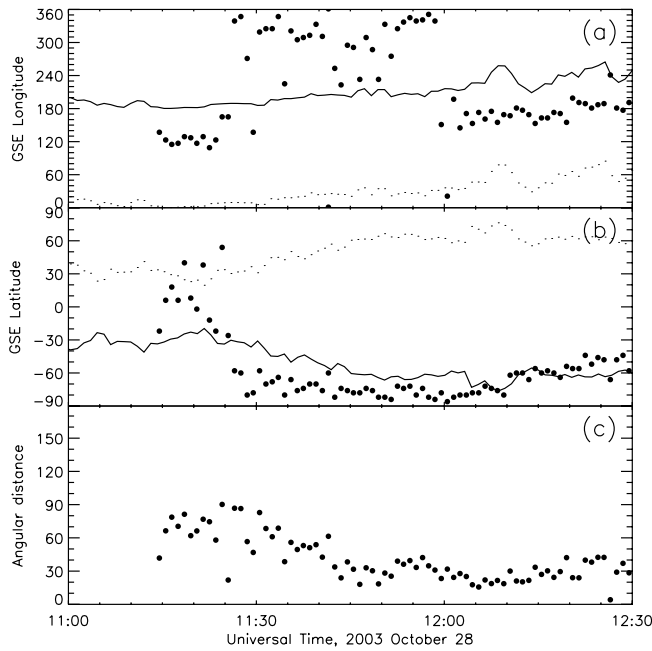


FIG. 4.— Axis of symmetry of arrival directions of relativistic solar protons (filled circles) in comparison with the magnetic field direction measured by the ACE spacecraft (solid line) and the antifield direction (dotted line) on 2003 October 28, in terms of (a) GSE longitude, (b) GSE latitude, and (c) angular separation between the axis of symmetry and magnetic field direction (all angles in degrees). The field direction was highly disturbed due to the recent passage of a previous coronal mass ejection; that disturbance, along with the large gyro-radius of the relativistic particles, could underlie the substantial deviation of the axis of symmetry from the field direction. Note that the jump in the longitude of the axis of symmetry at  $\approx 12:00$  UT corresponds to a smooth rotation across the south polar region.

stations. These are the 11 stations of the Spaceship Earth network (see Bieber et al. 2004 for details), supplemented by Terre Adelle and Barentsburg. Individual NM profiles first require a GCR background subtraction to infer the SEP contribution. Specifically, the SEP contribution is due to relativistic solar ions, dominated by protons, over a broad range of rigidity. The central 50% of the detector response was over 2.0–5.2 GV, for a spectral index of 4.2 as inferred from the South Pole bare counter to NM ratio (Bieber & Evenson 1991). Simulations were performed for protons at 10 representative rigidities corresponding to the 5th, 15th, . . . , 95th percentiles of the detector response. Following Bieber et al. (2005), we assumed a constant GCR count rate for an individual station throughout the event.

The background-subtracted profiles of the 13 polar NM stations are combined to produce the density, weighted anisotropy, and curvature profiles by fitting the intensity at each station's asymptotic viewing direction to a global function of angle with respect to an optimal axis of symmetry, which is shown in Figure 4. We can confirm an early SEP peak directed approximately sunward, at latitude  $\approx 0^\circ$  and longitude  $\approx 120^\circ$ , which agrees reasonably well with the direction reported by Miroshnichenko et al. (2005, their source 2). At 11:26 UT, the axis of symmetry we infer for the particle distribution jumped by about  $100^\circ$ , to latitude  $\approx -75^\circ$  and longitude  $\approx 315^\circ$  (to be compared with source 1 of Miroshnichenko et al. 2005 at latitude  $-59^\circ$  to  $-63^\circ$  and longitude  $253^\circ$  to  $260^\circ$  during 11:30–11:55 UT). This marks the start of a main peak directed roughly northward. In our data, the early peak and main peak are mainly distinguished by the particle flow direction, with distinct peak times in different monitors. The angular coverage of the polar neutron monitor network is not

sufficient to clearly indicate whether they represent two peaks in the omnidirectional particle density, or only one distribution that rotates in direction. The main peak was followed by an elevated SEP flux that was nearly constant until a Forbush decrease arrived after 06:00 UT on October 29. Actually, the GCR time profile is not precisely known, so the late-time SEP profile must be considered uncertain as well. Therefore, we perform fits only up to 12:30 UT, shortly after the main peak.

The first minutes of the density profile were dominated by the early peak detected at the Russian NM stations at Norilsk and Cape Schmidt. The absence of a simultaneous strong signal on most other stations of the Spaceship Earth network shows that this peak was produced by an extremely anisotropic beam of solar protons, and makes it difficult to precisely determine the density and anisotropy parameters during 11:14–11:25 UT, although it is apparent that the density of the early peak is several times lower than the main peak. For the present, we set aside the problematic early peak, using a linear interpolation for the data during this time period, and instead focus our analysis on the main peak.

We then apply the techniques of Ruffolo et al. (1998) and Bieber et al. (2002) to analyze the density, weighted anisotropy, and curvature profiles, shown as points with error bars in Figure 5. It is found that setting the spectral index of magnetic fluctuations  $q$  to 1.0 provides a reasonably accurate model of the pitch-angle distributions. We find an acceptable fit for configuration 1 (a standard Archimedean spiral), as shown in Figures 5a–5c. The fit is for an optimal scattering mean free path of  $\lambda = 0.9 \pm 0.1$  AU, and an optimal injection function that starts at about 11:00 ST ( $\pm 2$  minutes) and peaks at 11:44 ST ( $\pm 2$  minutes), where ST refers to the time at the Sun (which for electromagnetic emissions would be the time of detection at Earth in universal time, UT, minus 8 minutes). A similar result was also reported by Bieber et al. (2005) based on fits to the data up to a somewhat later time. The  $\chi^2$  of the fit is 573 for 444 degrees of freedom. The best fits for configurations 3 and 5 are qualitatively reasonable but quantitatively somewhat worse, with  $\chi^2$  values (degrees of freedom) of 799 (441) and 685 (443), respectively. Configuration 2 can also produce a qualitatively reasonable fit, although with a high  $\lambda$  value ( $2.4 \pm 0.2$  AU) and earlier injection, starting at about 10:51 ST  $\pm 2$  minutes and peaking at 11:31 ST  $\pm 4$  minutes. The  $\chi^2$  of the fit is 735 for 443 degrees of freedom. Note that we do not consider configuration 2 to be physically likely, but include this configuration for comparison with configurations 4 and 6.

Turning to configurations 4 and 6, Figures 5e–5l show fits to the data for transport along the far leg of a loop as suggested by Miroshnichenko et al. (2005). The fits are qualitatively unreasonable. It is effectively impossible to produce a good fit to the data for transport from the far leg of the loop; the rapid defocusing of the beam of SEPs (as shown in Fig. 3) produces a weighted anisotropy that is much too low even for the best fit. The  $\chi^2$  values (degrees of freedom) for best fits with configurations 4 and 6 are 2090 (444) and 2195 (442), respectively, or 3.6–3.8 times worse than for configuration 1. The value of the (parallel) scattering mean free path for the best fits (shown in Fig. 5) is  $\lambda = 6.8 \pm 0.4$  AU for both configurations 4 and 6. Contrary to what happens in the spiral configuration 2, in these cases a higher value of  $\lambda$  does not result in better fits. A higher  $\lambda$  does increase the initial dipole anisotropy  $\delta$ , but also produces a more negative  $\delta$  later on, created by the reflected pulse. The only factor that could make  $\delta$  remain high and positive for as long as it was observed would be a continuous and increasing SEP injection near the Sun; however, that would result in a SEP density profile greatly exceeding the data. Therefore, we conclude that models with transport

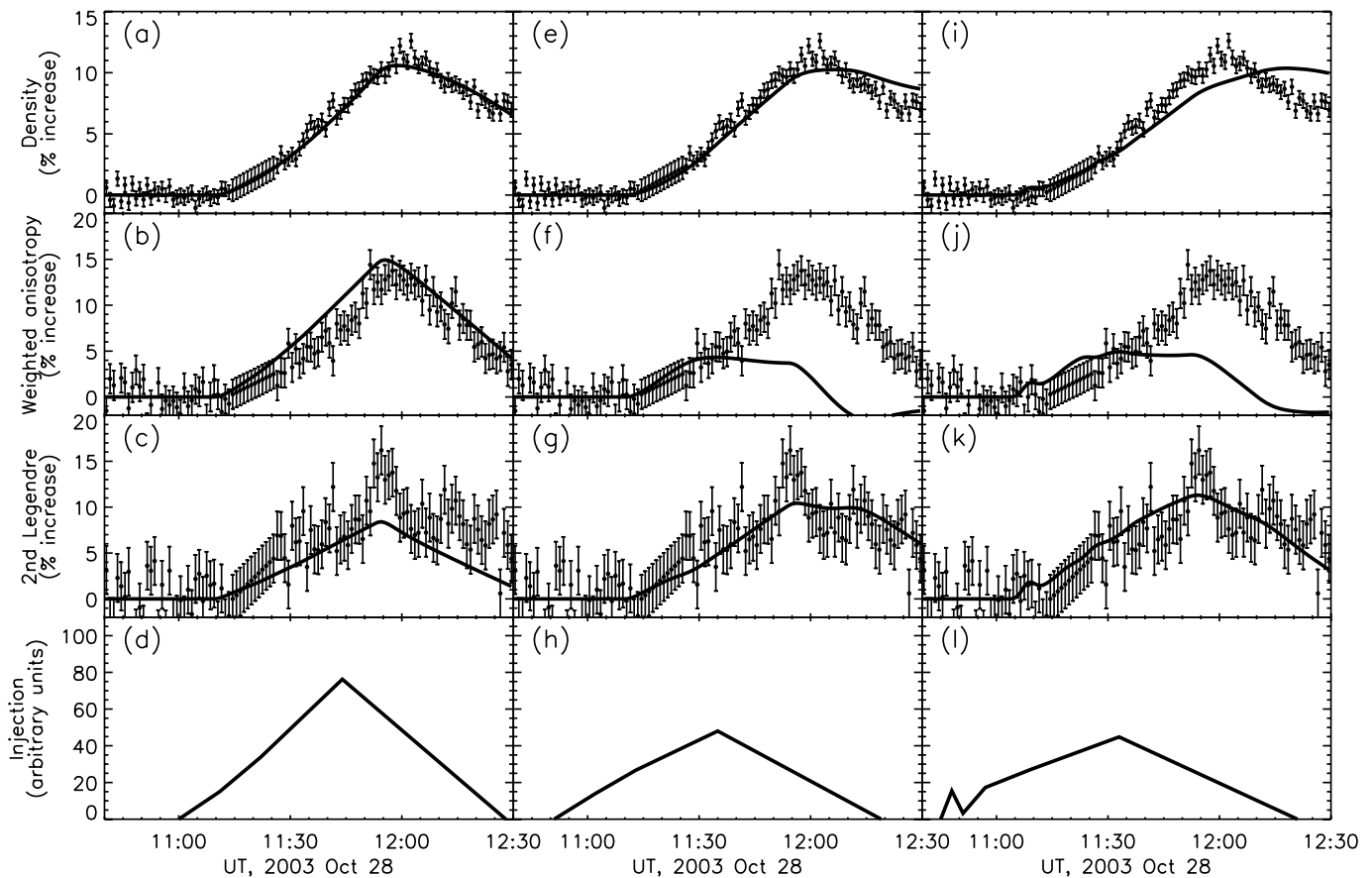


FIG. 5.—Panels (a)–(d): Best fit to (a) density, (b) weighted anisotropy, (c) second-order anisotropy (curvature) observations by polar neutron monitors, and (d) the inferred injection as a function of time at the Sun, for relativistic solar protons on 2003 October 28, assuming the spiral configuration 1 (see Fig. 1a). Panels (e)–(h): The same quantities using the loop configuration 4 with injection along the far leg (see Fig. 1d), which provides a substantially worse fit to the data. Panels (i)–(l): Results corresponding to the compressed loop configuration 6 with injection along the far leg (see Fig. 1f), similar to those for configuration 4.

along the far leg of a loop are unsuccessful in fitting observations of the main GLE peak of 2003 October 28.

## 5. DISCUSSION AND CONCLUSIONS

According to our results, when SEPs travel inside a closed interplanetary loop we can expect characteristic, direction-dependent (sunward or anti-sunward) signatures in their anisotropy distribution. The reverse focusing that the SEPs experience when they travel sunward past the Earth, i.e., coming from the far leg of a loop, will quickly reduce the dipole anisotropy. Furthermore, in the case of a very long mean free path, reflection due to mirroring near the Sun makes the dipole anisotropy become negative. In this sense, even a rare case of beam-like scatter-free transport cannot counterbalance the effects of reverse focusing (mirroring). Quantitative modeling confirms that the weighted anisotropy decays more rapidly than the SEP density for a wide range of mean free paths.

For the specific case of relativistic solar particles on 2003 October 28, observations of the main peak are quantitatively inconsistent with transport along the far leg of a loop (configurations 4 and 6). A model of transport along a very long spiral (configuration 2) gives acceptable quantitative fits to the data but is a physically unlikely scenario. We conclude that the main peak was produced by particles traveling either along an open spiral field line (configuration 1) or along the near leg of a loop (configuration 3 or 5).

The start time of particle injection at the Sun favored by configuration 1, with  $z = 1.03$  AU, is 11:00 ST ( $\pm 2$  minutes). This is consistent with the peak time of X-ray emission (11:02 ST), as found in previous quantitative modeling of three other relativistic proton events (Bieber et al. 2002, 2004; Ruffolo et al. 2006), and is somewhat later than the CME liftoff time estimates of 10:53 ST (linear fit) and 10:58 ST (quadratic fit)<sup>4</sup> and the onset of shock-related Type II radio emission at 10:54 ST,<sup>5</sup> allowing some time for shock acceleration to such high energies. In the long (2.2 AU) path length scenarios considered in this paper (which are either physically unreasonable or inconsistent with observations) the inferred start of the injection was 10:45 to 10:51 ST. This would be earlier than the times of the X-ray emission peak, CME liftoff, and the start of Type II radio emission. Such rapid injection would provide even more of a challenge to theories of shock acceleration of relativistic solar ions (see Manchester et al. 2005).

A path length of 2.2 AU for the main peak was inferred by Miroshnichenko et al. (2005) by means of an analysis of inverse

<sup>4</sup> Source: *Solar and Heliospheric Observatory (SOHO)*/Large Angle and Spectrometric Coronagraph Experiment CME catalog, available on the Web at [http://cdaw.gsfc.nasa.gov/CME\\_list](http://cdaw.gsfc.nasa.gov/CME_list). This CME catalog is generated and maintained by NASA and Catholic University of America in cooperation with the Naval Research Laboratory. *SOHO* is a project of international cooperation between ESA and NASA.

<sup>5</sup> Source: Space Environment Center. See [http://solar.sec.noaa.gov/ftpd/indices/2003\\_events/20031028events.txt](http://solar.sec.noaa.gov/ftpd/indices/2003_events/20031028events.txt).

velocities versus onset times. This employs a common assumption that the times of onset for different SEP energies are given by

$$t_{\text{onset}} = t_{\text{inj}} + \frac{z}{v}, \quad (14)$$

with  $v$  as the particle speed at each energy. This expression, based on a concept of scatter-free transport, can be used to fit  $t_{\text{onset}}$  versus  $1/v$  data, taking the time of injection  $t_{\text{inj}}$  and the path length  $z$  as free parameters. However, this method may lead to inferred path lengths that are too long, especially for a short mean free path or a high detection threshold (Sáiz et al. 2005). On the other hand, those authors found that the method is usually accurate to a few minutes for estimating the start time of injection, when data for relativistic particles are included.

In the case of relativistic ions on 2003 October 28, the path length inferred by Miroshnichenko et al. (2005) may have been influenced by details of the onset time analysis. For example, the  $t_{\text{inj}}$  value was constrained, reducing equation (14) to a one-parameter fit. Furthermore, the data used to determine onset times for *GOES* data of 80–165 MeV and 165–500 MeV (EPS instrument) were apparently uncorrected data, and the corrected data indicate onset times  $\sim 10$  minutes earlier.<sup>6</sup> Considering also the effect of interplanetary scattering (Lintunen & Vainio 2004; Sáiz et al. 2005), it is quite possible that the observed onset times of energetic ions were consistent with a path length of  $\sim 1$  AU from the Sun to the Earth along the guiding magnetic field.

We cannot precisely model the transport of particles arriving during the early peak on 2003 October 28, because the observation by only two high-latitude stations does not allow us to unambiguously determine the density and anisotropy parameters. Thus, we cannot rule out the early peak as due to particles coming from the far leg of a loop, although this would require a very intense and impulsive injection at a time earlier than 10:55 ST, i.e., earlier than the onset of neutron emission (Bieber et al. 2005; Watanabe et al. 2006). However, we can offer some additional insight based on our measured axis of symmetry (Fig. 4). Note that the direction of particle flow is offset from the magnetic field direction by roughly  $20^\circ$ – $90^\circ$ . An offset of up to  $\approx 60^\circ$  was observed for relativistic solar protons on 2000 July 14 (Bieber et al. 2002). This can be attributed to the large gyroradius; particles respond to the magnetic field averaged over a distance comparable to the turbulent correlation length ( $\sim 0.02$  AU), which does not necessarily coincide with the local field. On 2003 October 28, at the time of interest the magnetic field was especially disturbed due to the recent passage of a magnetic cloud, and the first detected particles are faster and have a higher gyroradius, which could account for the unusually large offset of up to  $90^\circ$  during both the early peak and the start of the main peak for this event.

<sup>6</sup> See <http://goes.ngdc.noaa.gov/>.

The remaining mystery is the sudden jump in the particle flow direction by  $\approx 100^\circ$  at 11:26 UT, marking the change from the early peak to the main peak (which are strong peaks at different neutron monitor stations viewing in different directions). The magnetic field was clearly highly disturbed (compared with the nominal Parker spiral direction of latitude  $0^\circ$  and longitude  $135^\circ$  or  $315^\circ$ ) and variable due to the recent passage of a magnetic cloud. It is possible that all the particles (including those in the early peak) came along an Archimedean spiral field or the near leg of a loop, and during the time of the early peak, 11:14–11:25 UT, the field lines of interest had a sharp bend by  $\sim 50^\circ$  (over a distance shorter than the particle gyroradius; see also Miroshnichenko et al. 2005) located sunward of Earth, causing the beam of particles to change direction by  $\sim 100^\circ$ . However, three-dimensional magnetic field information is not available to corroborate such speculation.

For a better understanding of the effects of the focusing length  $L$  (and its sign) on anisotropy signatures in the distribution of solar relativistic particles, we have also introduced a model of SEP transport within a compressed magnetic loop. In particular, a compression in the outermost portion of the loop is motivated by simulations of CMEs in the interplanetary medium (Vandas et al. 2002; Manchester et al. 2005). However, even when we place the observer in a region of sunward focusing (created by the compression) and assume particle injection along the far leg of the loop, we still find a rapid decline in the dipole anisotropy time profile not long after the SEP onset, and are unable to quantitatively fit the relativistic solar proton data for the main peak of 2003 October 28. The kink in the magnetic field near Earth as hypothesized by Miroshnichenko et al. (2005; see their Fig. 9) would have effects similar to such a compression, although with the addition of strong drifts perpendicular to the mean field.

In conclusion, SEPs can be detected within a closed interplanetary magnetic loop, but it is important to consider anisotropy signatures and other observable effects before inferring the existence of a loop configuration based on SEP observations. In particular, when energetic particles travel along the far leg of a loop and first reach the detector while moving sunward, the dipole anisotropy for an instantaneous injection declines rapidly with time, and the weighted anisotropy (anisotropy times density) should be observed to decline much more rapidly than the density. For an extended injection of particles, the maximum anisotropy remains rather low. A quantitative examination of the particle density and anisotropy can clearly distinguish between alternative magnetic configurations for which the particles have a different transport history and a different injection history.

This work was partially supported by the Mahidol University Postdoctoral Fellowship Program, the Thailand Research Fund, and NSF grant ATM-0527878. We wish to thank Kuntida Suwatharakunton, Nattapong Kamyun, and Maneenate Wechakama for their computational support.

## REFERENCES

- Bai, T. 1987, *ApJ*, 314, 795  
 Bame, S. J., Asbridge, J. R., Feldman, W. C., Gosling, J. T., & Zwickl, R. D. 1981, *Geophys. Res. Lett.*, 8, 173  
 Bieber, J. W., Clem, J., Evenson, P., Pyle, R., Ruffolo, D., & Sáiz, A. 2005, *Geophys. Res. Lett.*, 32, L03S02  
 Bieber, J. W., & Evenson, P. 1991, in *Proc. 22nd Int. Cosmic Ray Conf. (Dublin)*, 3, 129  
 Bieber, J. W., Evenson, P. A., Dröge, W., Pyle, R., Ruffolo, D., Rujiwarodom, M., Tooprakai, P., & Khumlumlert, T. 2004, *ApJ*, 601, L103  
 Bieber, J. W., et al. 2002, *ApJ*, 567, 622  
 Burlaga, L., Sittler, E., Mariani, F., & Schwenn, R. 1981, *J. Geophys. Res.*, 86, 6673  
 Buttighoffer, A. 1998, *A&A*, 335, 295  
 Buttighoffer, A., Lanzerotti, L. J., Thomson, D. J., MacLennan, C. G., & Forsyth, R. J. 1999, *A&A*, 351, 385  
 Cane, H. V. 1988, *J. Geophys. Res.*, 93, 1  
 Earl, J. A. 1973, *ApJ*, 180, 227  
 ———. 1976, *ApJ*, 205, 900  
 Hatzky, R., Kallenrode, M.-B., & Schmidt, J. M. 1997, in *Proc. 25th Int. Cosmic Ray Conf. (Durban)*, 1, 245

- Jokipii, J. R. 1971, *Rev. Geophys. Space Phys.*, 9, 27
- Kahler, S. W. 2005, *ApJ*, 628, 1014
- Kocharov, L. G., Torsti, J., Vainio, R., & Kovaltsov, G. A. 1996, *Sol. Phys.*, 165, 205
- Kocharov, L., Kovaltsov, G. A., Torsti, J., & Huttunen-Heikinmaa, K. 2005, *J. Geophys. Res.*, 110, A12S03
- Kocharov, L., Saloniemi, O., Torsti, J., Kovaltsov, G., & Riihonen, E. 2007, *ApJ*, 654, 1121
- Kocharov, L., Vainio, R., Kovaltsov, G. A., & Torsti, J. 1998, *Sol. Phys.*, 182, 195
- Lario, D., Sanahuja, B., & Heras, A. M. 1998, *ApJ*, 509, 415
- Lintunen, J., & Vainio, R. 2004, *A&A*, 420, 343
- Manchester, IV, W. B., et al. 2005, *ApJ*, 622, 1225
- Miroshnichenko, L. I., De Koning, C. A., & Pérez-Enríquez, R. 2000, *Space Sci. Rev.*, 91, 615
- Miroshnichenko, L. I., Klein, K.-L., Trotter, G., Lantos, P., Vashenyuk, E. V., Balabin, Y. V., & Gvozdevsky, B. B. 2005, *J. Geophys. Res.*, 110, A09S08
- Mulligan, T., Blake, J. B., Mazur, J. E., Quenby, J., & Shaul, D. 2005, in *Proc. 29th Int. Cosmic Ray Conf. (Pune)*, 1, 379
- Ng, C. K., & Wong, K.-Y. 1979, in *Proc. 16th Int. Cosmic Ray Conf. (Kyoto)*, 5, 252
- Nutaro, T., Riyavong, S., & Ruffolo, D. 2001, *Comp. Phys. Comm.*, 134, 209
- Palmer, I. D., Allum, F. R., & Singer, S. 1978, *J. Geophys. Res.*, 83, 75
- Parker, E. N. 1958, *ApJ*, 128, 664
- Reames, D. V., Ng, C. K., & Berdichevsky, D. 2001, *ApJ*, 550, 1064
- Richardson, I. G., & Cane, H. V. 1996, *J. Geophys. Res.*, 101, 27521
- Richardson, I. G., Dvornikov, V. M., Sdobnov, V. E., & Cane, H. V. 2000, *J. Geophys. Res.*, 105, 12579
- Roelof, E. C. 1969, in *Lectures in High Energy Astrophysics*, ed. H. B. Ögelman & J. R. Wayland, (NASA SP-199; Washington: NASA), 111
- Ruffolo, D. 1991, *ApJ*, 382, 688
- . 1995, *ApJ*, 442, 861
- Ruffolo, D., & Khumlumert, T. 1995, *Geophys. Res. Lett.*, 22, 2073
- Ruffolo, D., Khumlumert, T., & Youngde, W. 1998, *J. Geophys. Res.*, 103, 20591
- Ruffolo, D., Tooprakai, P., Rujiwarodom, M., Khumlumert, T., Wechakama, M., Bieber, J. W., Evenson, P., & Pyle, R. 2006, *ApJ*, 639, 1186
- Sáiz, A., Evenson, P. A., Ruffolo, D., & Bieber, J. W. 2005, *ApJ*, 626, 1131
- Torsti, J., Riihonen, E., & Kocharov, L. 2004, *ApJ*, 600, L83
- Vandas, M., Odstrčil, D., & Watari, S. 2002, *J. Geophys. Res.*, 107(A9), 1236
- Watanabe, K., et al. 2006, *ApJ*, 636, 1135
- Wilson, J. W., Goldhagen, P., Rafnsson, V., Clem, J. M., de Angelis, G., & Friedberg, W. 2003, *Adv. Space Res.*, 32, 3